# Development of a novel nitro-derivative of noscapine for the potential treatment of drug-resistant ovarian cancer and T-cell lymphoma

Ritu Aneja, Surya N. Vangapandu, Manu Lopus, Ramesh Chandra, Dulal Panda and Harish C. Joshi

Laboratory for Drug Discovery and Research, Department of Cell Biology (R.A., S.N.V., H.C.J.), Emory University School of Medicine, 615 Michael Street, Atlanta, GA 30322, USA; B. R. Ambedkar Center for Biomedical Research (R.C.), University of Delhi, India and School of Biosciences and Bioengineering, Indian Institute of Technology Bombay (M.L., D.P.), Mumbai, India.

Molecular Pharmacology Fast Forward. Published on March 3, 2006 as DOI: 10.1124/mol.105.021899
This article has not been copyedited and formatted. The final version may differ from this version.


a) Running Title: Novel treatment strategy for drug-resistant cancers

b) Corresponding Author: Harish C. Joshi, Department of Cell Biology, Emory University School of Medicine, Laboratory for Drug Discovery and Research, 615 Michael Street, Atlanta, GA 30322, USA

Phone: 404-727-0445, Fax: 404-727-6256, email: joshi@cellbio.emory.edu

c) Number of text pages: 28

Number of tables : 1

Number of figures: 4

Number of words in Abstract: 194

Number of words in the Introduction: 709

**Abbreviations**:

9-nitro-nos, 9-nitro-noscapine; TLC, thin layer chromatography; DMEM, Dulbecco's Modification of Eagle's Medium; PIPES, piperazine-*N*,*N*′-bis(2-ethanesulfonic acid); PBS, phosphate-buffered saline; BSA, bovine serum albumin; FITC, fluorescein isothiocyanate.

Molecular Pharmacology Fast Forward. Published on March 3, 2006 as DOI: 10.1124/mol.105.021899
This article has not been copyedited and formatted. The final version may differ from this version.


**Abstract**

We have previously shown that an antitussive plant alkaloid, noscapine binds tubulin, displays anticancer activity, and has a safe pharmacological profile in humans. Structure-function analyses pointed to a proton at position-9 of the isoquinoline ring that can be modified without compromising tubulin binding activity. Thus many noscapine analogs with different functional moieties at position-9 were synthesized. Those analogs that kill human cancer cells resistant to other anti-microtubule agents, *vincas* and *taxanes*, were screened. Here we present one such analog, 9-nitro-noscapine (9-nitro-nos), which binds tubulin and induces apoptosis selectively in tumor cells (ovarian and T-cell lymphoma) resistant to paclitaxel, vinblastine and teniposide. Surprisingly, 9-nitro-nos treatment at doses as high as 100 μM, did not affect the cell cycle profile of normal human fibroblasts. This selectivity of 9-nitro-nos for cancer cells represents a unique edge over the other available antimitotics. 9-nitro-nos perturbs the progression of cell cycle by mitotic arrest, followed by apoptotic cell death associated with increased caspase-3 activation and appearance of TUNEL-positive cells. Thus, we conclude that 9-nitro-nos has great potential to be a novel therapeutic agent for ovarian and T-cell lymphoma cancers, even those that have become drug-resistant to currently available chemotherapeutic drugs.

Microtubules are major cytoskeletal structures responsible for maintaining genetic stability during cell division (Sammak and Borisy, 1987). The dynamics of these polymers is absolutely crucial for this function that can be described as their growth rate at the plus ends, catastrophic shortening, frequency of transition between the two phases, pause between the two phases, their release from the microtubule organizing center and treadmilling (Kirschner and Mitchison, 1986; reviewed in Zhou and Giannakakou, 2005). Microtubule lattice also serves as tracks for the axonal transport of organelles driven by anteriograde and retrograde molecular motors to generate and maintain axonal integrity (Joshi, 1998). Interference with microtubule dynamics often leads to programmed cell death and thus microtubule-binding drugs are currently used to treat various malignancies in the clinic (Jordan and Wilson, 2004). Although useful, currently used microtubule drugs such as *vincas* and *taxanes* are limited due to the emergence of drug resistance. There have been multiple mechanisms for antimicrotubule drug resistance including overexpression of drug-efflux pumps, misexpression of tubulin isotypes, and perhaps mutational lesions in tubulin itself (Ranganathan et al., 1996; Giannakakou et al., 1997; Monzo et al., 1999; Dumontet et al., 2005).

The pharmacological profile of microtubule-binding agents, however, has not been ideal. Most of them need to be infused over long periods of time in the clinic because they are not water-soluble and can cause hypersensitive reactions due to the vehicle solution (Rowinsky, 1997). Furthermore, normally dividing cells within the healthy tissues such as intestinal crypts, hair follicles, and the bone marrow are also vulnerable to these agents leading to toxicities (Rowinsky, 1997). In addition, nerve cells dependent on molecular traffic over long distances undergo degenerative changes causing peripheral neuropathies (Pace et al., 1996; Crown and O'Leary, 2000; Theiss and Meller, 2000; Topp et al., 2000).

We have recently discovered that noscapine, a safe antitussive agent for over 40 years, binds tubulin, arrests dividing cells in mitosis and induces apoptosis (Ye et al., 1998). It is well-tolerated in humans and has been shown to be non-toxic in healthy volunteers including pregnant mothers (Dahlstrom et al., 1982; Karlsson et al., 1990; Jensen et al., 1992). Unlike the other microtubule-targeting drugs, noscapine does not significantly change the microtubule polymer mass even at high concentrations. Instead, it suppresses microtubule dynamics by increasing the time that microtubules spend in an attenuated (pause) state when neither microtubule growth nor shortening is detectable (Landen et al., 2002). Thus noscapine-induced suppression of microtubule dynamics, even though subtle, is sufficient to interfere with the proper attachment of chromosomes to kinetochore microtubules and to suppress the tension across paired kinetochores (Zhou et al., 2002a). This represents an improvement over the *taxanes*, the microtubule-bundling agents or overpolymerizers, and *vincas*, the depolymerizers, that cause toxicities in mitotic and

post-mitotic neurons at elevated doses. Noscapine thus effectively inhibits the progression of various cancer types both in cultured cells and in animal models with no obvious side effects (Ye et al., 1998; Landen et al., 2002, 2004; Zhou et al., 2002b; 2003). Surprisingly, the apoptosis is much more pronounced in cancer cells compared with normal healthy cells (Landen et al., 2002). Furthermore, we have done extensive structure-activity relationship studies producing a battery of analogs of which two analogs have shown potent activity against cancer cells without detectable toxicities (Checchi et al., 2003; Zhou et al., 2003, 2004, 2005a). The parent compound noscapine itself is also active against cancer cells including drug-resistant variants *al beit* at high concentrations.

In this study, we present the synthesis, characterization and an evaluation of the anti-tumor potential of a novel nitro analog of noscapine, 9-nitro-nos, which binds tubulin, effectively inhibits cell proliferation of 1A9 (ovarian cancer cells) and its paclitaxel-resistant variant (1A9/PTX22), and human lymphoblastoid cells CEM, and its vinblastine- (CEM/VLB100) and teniposide- (CEM/VM-1-5) resistant variants. 9-nitro-nos treatment selectively halts cell cycle progression at the G2/M phase in cancer cells without affecting the cell cycle of normal human fibroblast cells. This mitotic catastrophe in cancer cells is then followed by induction of apoptosis. The apoptotic mechanism is associated with activation of the key executioner cysteine protease, caspase-3. Most importantly, 9-nitro-nos is more potent against cancer cells that have become resistant to currently used drugs, like vinblastine, teniposide and paclitaxel as compared to their respective sensitive-parent lines.

## Materials and Methods

**Chemistry:** $^{1}H$ NMR and $^{13}C$ NMR spectra were measured by 400 NMR spectrometer in a $CDCl_3$ solution and analyzed by INOVA. Proton NMR spectra were recorded at 400 MHz and were referenced with residual chloroform (7.27 ppm). Carbon NMR spectra were recorded at 100 MHz and were referenced with 77.27 ppm resonance of residual chloroform. Abbreviations for signal coupling are as follows: s, singlet; d, doublet; t, triplet; q, quartet; m, multiplet. Infrared spectra were recorded on sodium chloride discs on Mattson Genesis II FT-IR. High resolution mass spectra were collected on Thermo Finnigan LTQ-FT Hybrid mass spectrophotometer using 3-nitrobenzyl alcohol or with addition of LiI as a matrix. Melting points were determined using a Thomas-Hoover melting point apparatus and were uncorrected. All reactions were conducted with oven-dried (125°C) reaction vessels in dry argon. All common reagents and solvents were obtained from Aldrich and were dried using 4 Å molecular sieves. The reactions were monitored by thin layer chromatography (TLC) using silica gel 60 F254 (Merck) on precoated aluminum sheets. Flash chromatography was carried out on standard grade silica gel (230-400 mesh).

**Synthesis of 9-nitro-nos:** To a solution of noscapine (4.134 g, 10 mmol) in acetonitrile (50 ml), silver nitrate (1.70 g, 10 mmol) and trifluoroacetic anhydride (5 ml, 35 mmol) were added. After one hour of reaction time, the reaction progress was monitored using thin layer chromatography (10% methanol in chloroform) and the reaction mixture was poured into 50 ml of water and extracted with chloroform (3 x 50 ml). The organic layer was washed with brine, dried over anhydrous magnesium sulfate and the solvent was evaporated *in vacuo*. The desired product, (*S*)-6,7-dimethoxy-3-((*R*)-4-methoxy-6-methyl-9-nitro-5,6,7,8-tetrahydro-[1,3]dioxolo[4,5-*g*]isoquinolin-5-yl)isobenzofuran-1(3*H*)-one (9-nitro-nos) was obtained as yellow crystalline powder by flash chromatography (silica gel, 230-400 mesh) with 10% methanol in chloroform as an eluent. mp 178.2-178.4°C; IR: 1529, 1362 $cm^{-1}$; $^{1}H$ NMR ($CDCl_3$, 400 MHz): δ 7.27 (d, 1H, *J* = 8.0 Hz), 7.08 (d, 1H, *J* = 8.0 Hz), 6.02 (s, 2H), 5.91 (d, 1H, *J* = 4.1 Hz), 4.42 (d, 1H, *J* = 4.1 Hz), 4.09 (s, 3H), 3.89 (s, 3H), 3.83 (s, 3H), 2.74-2.64 (m, 2H), 2.61-2.56 (m, 2H), 2.52 (s, 3H); $^{13}C$ NMR ($CDCl_3$, 100 MHz): δ 169.7, 157.2, 151.6, 147.5, 142.3, 140.5, 135.0, 134.2, 123.2, 120.8, 119.9, 119.4, 114.1, 100.8, 87.6, 63.7, 56.8, 56.4, 56.1, 51.4, 39.2, 27.0; HRMS (ESI): *m/z* Calcd. for $C_{22}H_{23}N_2O_9$ (M+1), 459.4821; Found, 459.4755 (M+1).

**HPLC Purity and Peak Attributions:**

The HPLC purity was determined following two different methods using varied solvent systems.

**Method 1**: Ultimate Plus, LC Packings, Dionex, $C_{18}$ column (pep Map 100, 3 µm, 100 Å particle size, ID: 1000 µm, length: 15 cm) with solvent systems A (0.1% formic acid in water) and B (acetonitrile), gradient, 25 min run at a flow of 40 µL/min. Retention time for 9-nitro-nos is 19.30 min. HPLC purity was 96%. **Method 2**: Ultimate Plus, LC Packings, Dionex, $C_{18}$ column (pep Map 100, 3 µm, 100 Å particle size, ID: 1000 µm, length: 15 cm) with solvent systems A (0.1% formic acid in water) and B (methanol), gradient, 25 min run at a flow of 40 µL/min. Retention time for 9-nitro-nos is 19.86 min. HPLC purity was 97%.

**Cell lines and chemicals:** Cell culture reagents were obtained from Mediatech, Cellgro. CEM, a human lymphoblastoid line, and its drug-resistant variants- CEM/VLB100 and CEM/VM-1-5, were provided by Dr. William T. Beck (Cancer Center, University of Illinois at Chicago). CEM-VLB100, a multi-drug resistant line selected against vinblastine is derived from the human lymphoblastoid line, CEM and expresses high levels of 170-kd P-glycoprotein (Beck and Cirtain, 1982). CEM/VM-1-5, resistant to the epipodophyllotoxin, teniposide (VM-26), expresses a much higher amount of MRP protein than CEM cells (Morgan et al., 2000). The 1A9 cell line is a clone of the human ovarian carcinoma cell line, A2780. The paclitaxel-resistant cell line, 1A9/PTX22, was isolated as an individual clone in a single-step selection, by exposing 1A9 cells to 5 ng/ml paclitaxel in the presence of 5 µg/ml verapamil, a P-glycoprotein antagonist (Giannakakou et al., 1997). All cells were grown in RPMI-1640 medium (Mediatech, Cellgro) supplemented with 10% fetal bovine serum (Invitrogen, Carlsbad, CA) and 1% penicillin/streptomycin (Mediatech, Cellgro). Paclitaxel-resistant 1A9/PTX22 cell line was maintained in 15 ng/ml paclitaxel and 5 µg/ml verapamil continuously, but was cultured in drug-free medium for 7 days prior to experiment. Human primary fibroblasts were cultured by digestion and trituration of prepuces of circumcised male babies. They were washed in sterile saline five times and cut up into small pieces prior to incubation with trypsin in Dulbecco's Modification of Eagle's Medium 1X (DMEM) for half an hour. Tissue clumps were removed and fibroblasts were plated onto culture dishes that were maintained at 37ºC and 5% $CO_2$ atmosphere in DMEM with 4.5 g/l glucose and L-glutamine (Mediatech, Cellgro) supplemented with 10% fetal bovine serum and 1% penicillin/streptomycin. Mammalian brain microtubule proteins were isolated by two cycles of polymerization and depolymerization and tubulin was separated from the microtubule binding proteins by phosphocellulose chromatography as described previously (Panda et al., 2000; Joshi and Zhou, 2001). The tubulin solution was stored at -80°C until use.

**Tubulin Binding Assay:** Fluorescence titration for determining the tubulin binding parameters was performed as described previously (Gupta and Panda, 2002). In brief, 9-nitro-nos (0-100 µM) was incubated with 2 µM tubulin in 25 mM PIPES, pH 6.8, 3 mM $MgSO_4$ and 1 mM EGTA for 45 min at

37°C. The relative intrinsic fluorescence intensity of tubulin was then monitored in a JASCO FP-6500 spectrofluorometer (JASCO, Tokyo, Japan) using a cuvette of 0.3-cm path length, and the excitation wavelength was 295 nm. The fluorescence emission intensity of 9-nitro-nos at this excitation wavelength was negligible. A 0.3-cm path-length cuvette was used to minimize the inner filter effects caused by the absorbance of 9-nitro-nos at higher concentration ranges. In addition, the inner filter effects were corrected using a formula $F_{corrected} = F_{observed} \cdot \text{antilog}\,[(A_{ex} + A_{em})/2]$, where $A_{ex}$ is the absorbance at the excitation wavelength and $A_{em}$ is the absorbance at the emission wavelength. The dissociation constant ($K_d$) was determined by the formula: $1/B = K_d/[\text{free ligand}] + 1$, where B is the fractional occupancy and [free ligand] is the concentration of free noscapine or 9-nitro-nos. The fractional occupancy (B) was determined by the formula $B = \Delta F/\Delta F_{max}$, where $\Delta F$ is the change in fluorescence intensity when tubulin and its ligand are in equilibrium and $\Delta F_{max}$ is the value of maximum fluorescence change when tubulin is completely bound with its ligand. $\Delta F_{max}$ was calculated by plotting $1/\Delta F$ versus 1/ligand using total ligand concentration as the first estimate of free ligand concentration.

**Tubulin Polymerization Assay:** Mammalian brain tubulin (1.0 mg/ml) was mixed with different concentrations of 9-nitro-nos (25 or 100 μM) at 0ºC in an assembly buffer (100 mM PIPES at pH 6.8, 3 mM $MgSO_4$, 1 mM EGTA, 1 mM GTP, and 1M sodium glutamate). Polymerization was initiated by raising the temperature to 37ºC in a water bath. The rate and extent of the polymerization reaction were monitored by light scattering at 550 nm, using a 0.3-cm path length cuvette in a JASCO FP-6500 spectrofluorometer (JASCO, Tokyo, Japan) for 30 minutes.

***In vitro* cell proliferation assays**

**Sulforhodamine B assay:** The cell proliferation assay was performed in 96-well plates as described previously (Skehan et al., 1990; Zhou et al., 2003). Adherent cells (1A9 and 1A9/PTX22) were seeded in 96-well plates at a density of $5 \times 10^3$ cells per well. They were treated with increasing gradient concentrations of 9-nitro-nos the next day while in log-phase growth. After 72 hours of drug treatment, cells were fixed with 50% trichloroacetic acid and stained with 0.4% sulforhodamine B dissolved in 1% acetic acid. Cells were then washed with 1% acetic acid to remove unbound dye. The protein-bound dye was extracted with 10 mM Tris base to determine the optical density at 564-nm wavelength.

**MTS assay:** Suspension cells (CEM, CEM/VLB100 and CEM/VM-1-5) were cultured in RPMI-1640 media containing 10% FBS and then seeded into 96-well plates at a density of $5 \times 10^3$ cells per well and were treated with increasing gradient concentrations of 9-nitro-nos for 72 hours. Measurement of cell proliferation was performed colorimetrically by 3-(4,5-dimethylthiazol-2-yl)-5-(3-

carboxymethoxyphenyl)-2-(4-sulphophenyl)-2H-tetrazolium, inner salt (MTS) assay, using the CellTiter96 AQueous One Solution Reagent (Promega, Madison, WI). Cells were exposed to MTS for 3 hours and absorbance was measured using a microplate reader (Molecular Devices, Sunnyvale, CA) at an optical density (OD) of 490 nm. The percentage of cell survival as a function of drug concentration for both the assays was then plotted to determine the $IC_{50}$ value, which stands for the drug concentration needed to prevent cell proliferation by 50%.

**Cell cycle analysis:** The flow cytometric evaluation of the cell cycle status was performed as described previously (Zhou et al., 2003). Briefly, 2 x $10^6$ cells were centrifuged, washed twice with ice-cold PBS, and fixed in 70% ethanol. Tubes containing the cell pellets were stored at 4ºC for at least 24 hours. Cells were then centrifuged at 1000 x g for 10 min and the supernatant was discarded. The pellets were washed twice with 5 ml of PBS and then stained with 0.5 ml of propidium iodide (0.1% in 0.6% Triton-X in PBS) and 0.5 ml of RNase A (2 mg/ml) for 45 minutes in dark. Samples were then analyzed on a FACSCalibur flow cytometer (Beckman Coulter Inc., Fullerton, CA).

**Immunofluorescence microscopy:** Cells adhered to poly-L-lysine coated coverslips were treated with 9-nitro-nos for 72 hours. After treatment, cells were fixed with cold (-20ºC) methanol for 5 min and then washed with phosphate-buffered saline (PBS) for 5 min. Non-specific sites were blocked by incubating with 100 μl of 2% BSA in PBS at 37ºC for 15 min. A mouse monoclonal antibody against α-tubulin (DM1A, Sigma) was diluted 1:500 in 2% BSA/PBS (100 μl) and incubated with the coverslips for 2 hours at 37ºC. Cells were then washed with 2% BSA/PBS for 10 min at room temperature before incubating with a 1:200 dilution of a fluorescein-isothiocyanate (FITC)-labeled goat anti-mouse IgG antibody (Jackson ImmunoResearch, Inc., West Grove, PA) at 37ºC for 1 hour. Coverslips were then rinsed with 2% BSA/PBS for 10 min and incubated with propidium iodide (0.5 μg/ml) for 15 min at room temperature before they were mounted with Aquamount (Lerner Laboratories, Pittsburgh, PA) containing 0.01% 1,4-diazobicyclo(2,2,2)octane (DABCO, Sigma). Cells were then examined using confocal microscopy for microtubule morphology, and nuclear morphology to visualize DNA fragmentation (at least 100 cells were examined per condition).

**Terminal Deoxynucleotidyl-Transferase-Mediated dUTP Nick-End Labeling (TUNEL) Assay for Apoptosis:** DNA strand breaks were identified by using the TUNEL assay as described (Bortner et al., 1995). In brief, 1A9/PTX22 cells were incubated with 50 μM 9-nitro-nos for 72 hours. Cells were pelleted and washed with ice-cold PBS twice. Cells were then fixed in 1% paraformaldehyde, and apoptosis was detected using the APO-BrdU TUNEL Assay Kit from Molecular Probes (Eugene, OR) according to the manufacturer's instructions. Breifly, cells were stained for a flow cytometry-based terminal

deoxynucleotidyl transferase (TdT)-mediated bromo-deoxyuridine triphosphate (BrdUTP) reaction. Addition of BrdUTP to the TdT reaction provides a means to label the DNA strand breaks and is detected by an Alexa Fluor 488 labeled anti-BrdU antibody. DNA content was determined by the binding of DNA specific dye, propidium iodide (x-axis). Apoptotic cells were determined by incorporation of BrdU at the 3′-OH ends of the fragmented DNA as measured by anti-BrdU Alexa Fluor 488 labeled antibody on the y-axis. Number of apoptotic cells is indicated by the number of Alexa Fluor 488 positive cells of the total gated cells. This assay was run on a flow cytometer equipped with a 488 nm argon laser as the light source. PI fluoresces at about 623 nm and Alexa-Fluor 488 at about 520 nm when excited at 488 nm. Single and dual parameter displays were created using the Cell Quest Data Acquisition Software (Becton Dickinson). The gating display was the standard dual parameter DNA doublet discrimination display with the DNA area signal on the Y-axis and the DNA width signal on the X-axis. From this display, a gate was generated around the non-clumped cells and the second gated dual parameter display was generated with the DNA (linear red fluorescence) on the X-axis and the Alexa-Fluor 488 (log green fluorescence) on the Y-axis. Apoptotic cells were subsequently counted as those expressing high Alexa-Fluor 488 fluorescence. Confocal micrographs were also obtained for the TUNEL-stained cells using a 63X objective with a numerical aperture of 1.4.

**Determination of caspase-3 activity:** $10^6$ cells were incubated with 25 μM 9-nitro-nos (CEM, CEM/VLB100 and CEM/VM-1-5) or 50 μM 9-nitro-nos (1A9 and 1A9/PTX22) for 0, 24, 48 and 72 hours. Caspase-3 activity was then measured by the cleavage of the small synthetic substrate Z-DEVD-aminoluciferin (CaspaseGloTM 3/7 Assay System Kit, Promega, Madison, WI) that becomes luminogenic upon cleavage. The luminescent signal, which is directly proportional to the amount of caspase-3 activity, was measured in a Luminoscan Ascent instrument from ThermoLab systems, following an incubation of 3 hours.

Molecular Pharmacology Fast Forward. Published on March 3, 2006 as DOI: 10.1124/mol.105.021899
This article has not been copyedited and formatted. The final version may differ from this version.


## Results

The nitration reaction is a well-studied electrophilic substitution reaction in organic chemistry. Although, fuming nitric acid or 50% nitric acid in glacial acetic acid are extensively used for obtaining the nitrated product, the harsh oxidizing conditions of these reagents did not allow us to use these reagents for the nitration of noscapine. The lead compound, noscapine comprises of isoquinoline and benzofuranone ring systems joined by a labile C-C chiral bond and both these ring systems contain several vulnerable methoxy groups. Thus, achieving selective nitration at C-9 position without disruption and cleavage of these labile groups and C-C bonds was challenging. Treatment of noscapine with other nitrating agents like acetyl nitrate or benzoyl nitrate also resulted in epimerization or diastereoisomers (Lee, 2002). Next, we tried inorganic nitrate salts like ammonium nitrate or silver nitrate in the presence of acidic media to achieve aromatic nitration (Crivello, 1981). After carefully titrating several conditions and reagents, we successfully accomplished the nitration of noscapine using trifluoroacetic anhydride (TFAA). TFAA represents another commonly employed reagent and its extensive use is associated with its ability to generate a mixed anhydride, trifluoroacetyl nitrate that is a reactive nitrating agent (Crivello, 1981). We also tried other reagents such as ammonium nitrate, sodium nitrate or silver nitrate in chloroform but those gave us low quantitative yields and had longer reaction times. Increased reaction rate and yields were obtained using a lower dielectric constant solvent, acetonitrile. The reaction was slightly exothermic and completed in one hour. The product remained in solution while the inorganic salt of trifluoroacetic acid precipitated and was removed by filtration.

Thus, (*S*)-6,7-dimethoxy-3-((*R*)-4-methoxy-6-methyl-9-nitro-5,6,7,8-tetrahydro-[1,3]dioxolo[4,5-*g*]isoquinolin-5-yl)isobenzofuran-1(3*H*)-one (9-nitro-nos) was prepared by the aromatic nitration of (*S*)-6,7-dimethoxy-3-((*R*)-4-methoxy-6-methyl-5,6,7,8-tetrahydro-[1,3]dioxolo[4,5-*g*]isoquinolin-5-yl)isobenzofuran-1(3*H*)-one (noscapine) using silver nitrate in acetonitrile and TFAA at 25°C (Figure 1A). This method resulted in controlling the chemoselectivity of the reaction, in that aromatic substitution occurred at C-9 position of ring A of the isoquinoline nucleus. Absence of C-9 aromatic proton at δ 6.52-ppm in the $^{1}$H NMR spectrum of the product confirmed the nitration at C-9 position. Furthermore, $^{13}$C NMR and HRMS data confirmed the structure of the compound.

### 9-nitro-nos binds tubulin

Introduction of a nitro moiety in place of a proton usually disrupts the tight interactions within the ligand-binding pockets of proteins. Therefore, we first asked if this novel compound, 9-nitro-nos, retains the tubulin binding activity of the parent compound, noscapine. Tubulin, like many other proteins, contains

fluorescent amino acids like tryptophans and tyrosines. The intensity of the fluorescence emission is dependent upon the micro-environment around these amino acids in the folded protein. Agents that bind tubulin typically change the micro-environment and alter the fluorescent properties of the target protein (Ye et al., 1998; Peyrot et al., 1992; Panda et al., 1997). Measuring these fluorescent changes has become a standard method for determining the binding properties of tubulin ligands including the classical compound colchicine (Peyrot et al., 1989; Andreu et al., 1991). We thus used this standard method to determine the dissociation constant ($K_d$) between tubulin and 9-nitro-nos as compared to the carrier vehicle (DMSO). Our results show that 9-nitro-nos quenched tubulin fluorescence in a saturable manner (Figure 1B) and the double-reciprocal plot of these data revealed a $K_d$ of 86 ± 6 μM for 9-nitro-nos binding to tubulin (Figure 1C).

**9-nitro-nos does not affect the assembly rate and steady state monomer/polymer tubulin mass**

We next asked if 9-nitro-nos promoted or inhibited microtubule polymerization. We have previously shown that noscapine does not significantly promote or inhibit microtubule polymerization upon binding tubulin, even at a concentration as high as 100 μM (Zhou et al., 2003). However, it does alter the steady-state dynamics of microtubule assembly, primarily by increasing the amount of time that the microtubules spend in an attenuated (pause) state (Zhou et al., 2002a). This property of noscapine makes it unique and has resulted in its extensive use to explore the role of microtubule dynamics during the spindle assembly checkpoint signaling. More importantly, it provides an advantage that post-mitotic cells like neurons do not get adversely affected by this drug even at higher concentrations. This is in contrast to the currently used anticancer drugs such as the family of taxanes and the vinca alkaloids, high micromolar concentrations of which cause devastating effects on cellular microtubules. We thus examined the effect of 9-nitro-nos on the assembly of tubulin subunits into microtubules *in vitro* by measuring the changes in the turbidity produced upon tubulin polymerization. Our results show that 9-nitro-nos did not inhibit the rate or extent of tubulin polymerization at 25 μM or even at concentrations as high as 100 μM (Figure 1D). Having identified tubulin as the target molecule, we extended our pharmacology study at the cellular level to determine mechanisms by which 9-nitro-nos affects the cell cycle and induces cell death.

**9-nitro-nos effectively inhibits proliferation of cancer cells including vinblastine-, teniposide-, and paclitaxel- resistant variants**

Although many microtubule-binding drugs are active against many tumor types, most of these agents fail to manage the drug-resistant phenotypes of recurrent tumors. The NCI-60 cell panel shows a wide range of sensitivity for the parent compound noscapine, the drug-resistant variants, however, have not been fully

explored. One major mechanism of acquired drug resistance is the overexpression of efflux pumps, namely, P-gp170/MDR and MRP. For example, CEM/VLB100 cells, the pgp-overexpressing vinblastine-resistant variants show a 270-fold resistance to vinblastine (Beck and Cirtain, 1982) and CEM/VM-1-5 cells, the MRP-overexpressing variants display a 400-fold resistance to teniposide (Morgan et al., 2000). Surprisingly, 9-nitro-nos is active against the parental CEM cells and those of CEM-derived vinblastine- and teniposide- resistant cells despite pgp or MRP overexpression. We used an *in vitro* cell proliferation MTS assay to determine the drug concentration required to inhibit cell growth by 50% after incubation in the culture medium for 72 hours. Our results show that the median inhibitory concentration ($IC_{50}$) of 9-nitro-nos for CEM, CEM/VLB100 and CEM/VM-1-5 cells is 10 μM, 8.1 μM and 6.9 μM respectively (Figure 2). It is worth mentioning that the $IC_{50}$ value for the drug-resistant sub-lines is lower than the parent line.

We next examined the effect of 9-nitro-nos on ovarian cancer cells, 1A9 and its paclitaxel-resistant variant, 1A9/PTX22 (Giannakakou et al., 1997). Using a standard sulforhodamine B assay to evaluate percent cell survival for these adherent cells, we found the $IC_{50}$ value to be 30.1 μM and 27.5 μM for 1A9, the parent ovarian cancer cells and 1A9/PTX22, the paclitaxel-resistant variant, respectively (Figure 2). In the ovarian cancer cells also, we found that the $IC_{50}$ value for the drug-resistant variant was lower than the parent cells. Like other microtubule-binding drugs, such as taxanes and epothilones, 9-nitro-nos is also quite effective against drug-resistant cells. Though the 1A9/PTX22 cells do not overexpress Pgp rather have tubulin mutations that confers paclitaxel resistance, it is however, expected for 9-nitro-nos to display sensitivity towards drug-resistant cells owing to a different binding pocket. 9-nitro-nos has also been submitted by our laboratory for testing by the National Cancer Institute (NCI), through its Developmental Therapeutics Program (DTP), against their panel of 60 human cancer cell lines.

**9-nitro-nos alters cell cycle profile and induces G2/M arrest in cancer cells**

Microtubule-interfering agents, including noscapine (Ye et al., 1998; Zhou et al., 2002a) are well-known to arrest cell cycle progression at the G2/M phase in mammalian cells (Jordan and Wilson, 1999). Therefore, we next examined the effect of 9-nitro-nos on the percent G2/M and sub-G1 cell populations of these cancer cells as a function of time. As can be seen in Figure 3A, mitotic figures peak at about 24-48 hours of drug exposure and then decline up to 72 hours of observation. Consistent with this, the apoptotic cells rise in number during this time (Figure 3B). Fluorescently labeled DNA accumulation is a good indicator of cell cycle progression and cell death. An unreplicated complement of 2N DNA cells represents the G1 phase while duplicated 4N DNA cells represent G2 and M phases. Cells in the process of DNA duplication between 2N and 4N peaks represent the S phase. Less than 2N DNA appears in

populations of dying cells that degrade their DNA to different extents. Figure 3(C-G) depict the flow cytometric profile of CEM, CEM/VLB100, CEM/VM-1-5, 1A9, 1A9/PTX22 cells, respectively, treated with 9-nitro-nos for 0, 24, 48 and 72 hours. Twenty five micromolar 9-nitro-nos is used to study cell cycle profile in CEM, CEM/VLB1000 and CEM/VM-1-5 cells, whereas, fifty micromolar 9-nitro-nos is used for 1A9 and 1A9/PTX22 cells. As is clearly evident from the three-dimensional FACS profiles, the display of DNA content as a function of time of drug exposure shows pronounced increase in the population of cells that accumulate with less than 2N DNA (sub-G1 population) at 72 hours indicating dying cells. This is preceded by an accumulation of cell populations with 4N DNA indicating G2/M arrest. The anticancer activity of 9-nitro-nos treatment was thus evident in its ability to produce a significant sub-G1 population, representing the fraction of cells which have hypodiploid (< 2N) DNA content, typifying a cell population having degraded DNA, a characteristic of apoptosis. The effect of 9-nitro-nos on the progression of the entire cell cycle as a function of time shown as the percentage of G0/G1, S, G2/M and sub-G1 populations in all three lymphoma cell lines and the two ovarian cell lines is shown in Table 1.

Since the progression of normal cells through the cell cycle is tightly regulated by checkpoints, ensuring exact replication of the genome during the S-phase and its precisely equal division at mitosis, we investigated whether 9-nitro-nos affects the cell cycle of the normal human fibroblast cells. Surprisingly, we did not observe any perturbations in the cell cycle profile of normal fibroblast cells at even 100 μM 9-nitro-nos (Figure 3H). It is surprising that 9-nitro-nos did not affect the cell cycle profile of human fibroblasts while it did affect the cell cycle of primary melanocytes (Landen et al, 2002). Several possibilities exist. The first obvious possibility is that the primary fibroblasts are dormant, thus are not dividing. We do know, however, that these cells divide with a doubling time of about 18-20 hours. The second very likely possibility comes from an astute observation by Rieder and colleagues (Mikhailov A, et al., 2002), in which the authors make a clear case that cells in early stages of chromosome condensation (prometaphase) are reversible, in that drug-induced perturbations of microtubules can return cells from prometaphase to G2 phase. The mechanism of this reversal is not well-understood and several laboratories including ours are investigating this intriguing observation. Thus, our *in vitro* studies with normal human cell cultures that show resistance to the apoptotic effects of 9-nitro-nos are in contrast to the adverse effects seen with human cancer cells.

Nevertheless, the cell cycle analyses suggest that the lymphoma and the ovarian cancer cells including their drug-resistant variants succumb to apoptosis upon treatment with 9-nitro-nos. Therefore, we went on

to examine a variety of apoptotic events using several complementary cytometric and biochemical methods.

**9-nitro-nos causes extensive apoptosis as revealed by immunocytochemistry**

The onset of apoptosis characteristically changes cellular morphology. This includes membrane blebbing, formation of apoptotic bodies, disruption of cytoskeleton, and hypercondensation and fragmentation of chromatin. To visualize this, control untreated cells as well as cells treated with 9-nitro-nos for 72 hours were analyzed by immunocytochemistry using a tubulin-specific antibody (green) and a DNA-binding dye (red). Confocal micrographs (Figure 4A, top panel) shows control untreated CEM, CEM/VLB100, CEM/VM-1-5, 1A9 and 1A9/PTX22 cells. As expected, untreated control cells show normal radial microtubule arrays. In contrast, both lymphoma cells and ovarian cancer cells treated with 9-nitro-nos for 72 hours show extensive terminal apoptotic figures with fragmented DNA pieces and perturbed microtubule arrays (Figure 4A, bottom panels).

**9-nitro-nos treatment caused DNA fragmentation as measured quantitatively by a flow cytometry based TUNEL analysis**

To further establish the apoptotic mechanism of cell death quantitatively, we next performed a flow cytometry based TUNEL assay in 1A9/PTX22 cells treated with 9-nitro-nos for 72 hours. Since the end stages of apoptosis display cleaved 3´-ends of DNA, they can be visualized by specific labeling using TUNEL assay as an abundant green staining (Figure 4B, upper right panel, *open arrowheads*, red denotes PI staining). The quantitative FACS analysis showed 55.9% TUNEL-positive cells within a population of 1A9/PTX22 cells treated with 50 μM 9-nitro-nos for 72 hours (Figure 4B, upper left panel). In contrast, control untreated cells only occasionally show TUNEL-staining and TUNEL-negative cells appear red (Figure 4B, lower right panel, *solid arrowhead*). This is consistent with the quantitative FACS data that depict 95.9% control cells containing intact genomic DNA in the lower region of the cytogram representing the TUNEL-negative cells (Figure 4B, lower left panel). The other cell lines also showed similar results (data not shown). Although we do not know the precise mechanisms of the initial events that trigger apoptosis, however, we have shown the terminal stages by quantitating the 3’ ends of fragmented DNA as an evidence of the execution phase of apoptosis.

**9-nitro-nos causes activation of caspase-3, a hallmark of apoptosis, as a function of time**

Caspases, the cysteine proteases have been implicated as key participants in the sequence of events that result in the dismantling of the cell during apoptosis. The activation of caspase-3 is caused by upstream

caspases and involves the cleavage of the inactive proenzyme into an active form. The active form can be monitored using a small peptide substrate which becomes luminogenic upon cleavage. As shown in Figure 4C, we observed a concomitant time-dependent activation of caspase-3 as much as 10-20 fold in both the lymphoma cells and ovarian cancer cells including their drug-resistant variants upon 72 hours of 9-nitro-nos treatment. It is appreciated that the kinetics of caspase-3 activation depends very much upon the nature of stimuli and the timing of misbalance in pro-apoptotic and anti-apoptotic signals. As we have published earlier (Ye et al., 2001), it requires a long time of elevated p34cdc2 activity followed by the activation of JNK pathway prior to caspase activation and apoptosis. Antimicrotubule drug induced caspase induction also somewhat depends on the generation time of cells. The cell lines we used had a doubling time ranging from about 20 hours to 48 hours. This is perfectly in line with our hypothesis that p34cdc2 activation in G2/M block at about 24 hours is sustained for about 20 hours (perhaps due to a rather strong mitotic checkpoint) prior to the activation of stress activated kinases such as JNK. Although, a direct and precise correlation between the generation time and caspase activation is difficult to derive, however, the timing of the appearance of TUNEL-stained cells can be directly correlated with the timing of caspase activation burst.

Molecular Pharmacology Fast Forward. Published on March 3, 2006 as DOI: 10.1124/mol.105.021899
This article has not been copyedited and formatted. The final version may differ from this version.


## Discussion

Microtubule-interacting agents, both those that polymerize and bundle microtubules (such as *taxanes*), and depolymerize them decreasing polymer mass (such as *vincas*) have been useful for the treatment of many cancer types. Unfortunately, the clinical success of these agents has been severely hampered by the emergence of drug resistance. Although patients show significant response to these drugs during treatment, most relapse and fail to respond to the same drug at a later stage. Multidrug resistance, by which cancer cells quite often become resistant to many structurally and mechanistically unrelated drugs, thus makes successful chemotherapy more complex and difficult to achieve (Gottesman, 2002). This phenomenon is primarily due to an enhanced efflux of drugs from the inside to the outside of cells by drug pumps, a family of ABC transporter proteins located on the cell membrane. P-glycoprotein, for example, is one such drug pump and is encoded by the multidrug resistance 1 gene. Overexpression of P-glycoprotein has been found to affect drug accumulation in the cell and correlates with the multidrug resistance phenotype in cancer cells (Gottesman and Pastan, 1993). Altered expression of tubulin isotypes is another contributing mechanism towards drug resistance (Burkhart et al., 2001) besides other unknown mechanisms. Another major challenge to successful chemotherapy by these antimicrotubule agents is associated toxicity. This is mainly because microtubules perform many other functions such as cytoplasmic organization and axonal transport, besides their function in chromosome movement during mitosis. Since the microtubule-targeting drugs currently in use either promote excessive stability of microtubules, such as the taxane family, or induce depolymerization of microtubules like the vinca alkaloids, their usage is associated with various toxicities, such as gastrointestinal toxicity, alopecia, and peripheral neuropathy. A coupled aspect of the toxicity manifestation is their lack of specificity for dividing cells. Therefore, there has been a tremendous interest in identifying novel antimicrotubule agents that overcome various modes of resistance, display selectivity for cancer cells and have safer pharmacology profiles.

Our laboratory discovered that noscapine is a unique antimicrotubule drug that alters microtubule dynamics without affecting the total polymer mass of tubulin and can be successfully employed for probing the spindle assembly checkpoint mechanisms (Zhou et al., 2002a). In this study, we demonstrate that a nitro analog of noscapine, 9-nitro-nos effectively inhibits cellular proliferation of lymphoma and ovarian cancer cells, in particular, those that overexpress multidrug resistant proteins. Furthermore, 9-nitro-nos significantly arrest cells at the G2/M phase of the cell cycle followed by apoptotic cell death, as revealed by several prototypic features of apoptosis. Interestingly, unlike currently used chemotherapeutics, 9-nitro-nos does not affect the cell cycle of normal human fibroblast cells. These

Molecular Pharmacology Fast Forward. Published on March 3, 2006 as DOI: 10.1124/mol.105.021899
This article has not been copyedited and formatted. The final version may differ from this version.


findings thus indicate a great potential for the use of 9-nitro-nos as a chemotherapeutic agents for the treatment of human cancers, especially for those that are resistant to currently used microtubule drugs.

Molecular Pharmacology Fast Forward. Published on March 3, 2006 as DOI: 10.1124/mol.105.021899
This article has not been copyedited and formatted. The final version may differ from this version.


**Acknowledgements**

We thank Dr. William Beck for providing various CEM and its drug-resistant sublines used in this study and advice. We thank members of the Joshi laboratory for discussions. We are indebted to the anonymous reviewers of this manuscript for helpful suggestions.

## References

Andreu JM, Gorbunoff MJ, Medrano FJ, Rossi M and Timasheff SN (1991) Mechanism of colchicine binding to tubulin. Tolerance of substituents in ring C' of biphenyl analogues. *Biochemistry* 30:3777-3786.

Beck WT and Cirtain MC (1982) Continued expression of vinca alkaloid resistance by CCRF-CEM cells after treatment with tunicamycin or pronase. *Cancer Res* 42:184-189.

Bortner CD, Oldenburg NBE, Cidlowski JA (1995) The role of DNA fragmentation in apoptosis. *Trends Cell Biol* 5:21–26.

Burkhart CA, Kavallaris M, and Horwitz SB (2001) The role of beta-tubulin isotypes in resistance to antimitotic drugs. *Biochim Biophys Acta* 1471:1–9.

Crown J and O'Leary M (2000) The taxanes: an update. Lancet 355:1176–1178.

Checchi PM, Nettles JH, Zhou J, Snyder JP, Joshi HC (2003) Microtubule-interacting drugs for cancer treatment. *Trends Pharmacol Sci* 24:361-365.

Crivello JV (1981) Nitrations and oxidations with inorganic nitrate salts in trifluoroacetic anhydride. *J Org Chem* 46:3056-3060.

Crown J and O'Leary M (2000) The taxanes: an update. *Lancet* 355:1176-1178.

Dahlstrom B, Mellstrand T, Lofdahl CG and Johansson M (1982) Pharmacokinetic properties of noscapine. *Eur J Clin Pharmacol* 22:535-539.

Dumontet C, Isaac S, Souquet PJ, Bejui-Thivolet F, Pacheco Y, Peloux N, Frankfurter A, Luduena R and Perol M (2005) Expression of class III beta tubulin in non-small cell lung cancer is correlated with resistance to taxane chemotherapy. *Bull Cancer* 92:E25-30.

Giannakakou P, Sackett DL, Kang YK, Zhan Z, Buters JT, Fojo T and Poruchynsky MS (1997) Paclitaxel-resistant human ovarian cancer cells have mutant beta-tubulins that exhibit impaired paclitaxel-driven polymerization. *J Biol Chem* 272:17118-17125.

Gottesman MM (2002) Mechanisms of cancer drug resistance. *Annu Rev Med* 53:615-627

Gottesman MM and Pastan I (1993) Biochemistry of multidrug resistance mediated by the multidrug transporter. *Annu Rev Biochem* 62:385–427.

Gupta K and Panda D (2002) Perturbation of microtubule polymerization by quercetin through tubulin binding: a novel mechanism of its antiproliferative activity. *Biochemistry* 41:13029-13038.

Jensen LN, Christrup LL, Jacobsen L, Bonde J and Bundgaard H (1992) Relative bioavailability in man of noscapine administered in lozenges and mixture. *Acta Pharm Nord* 4:309-312.

Jordan MA and Wilson L (1999) The use and action of drugs in analyzing mitosis. *Methods Cell Biol* 61:267-291.

Jordan MA and Wilson L (2004) Microtubules as a target for anticancer drugs. *Nat Rev Cancer* 4:253-265.

Joshi HC (1998) Microtubule dynamics in living cells. *Curr Opin Cell Biol* 10:35-44.

Joshi HC and Zhou J (2001) Gamma tubulin and microtubule nucleation in mammalian cells. *Methods Cell Biol* 67:179-193.

Karlsson MO, Dahlstrom B, Eckernas SA, Johansson M and Alm AT (1990) Pharmacokinetics of oral noscapine. *Eur J Clin Pharmacol* 39:275-279.

Kirschner M and Mitchison TJ (1986) Beyond self-assembly: From microtubules to morphogenesis. *Cell* 45:329-342.

Landen JW, Hau V, Wang MS, Davis T, Ciliax B, Wainer BH, Van Meir E,G, Glass JD, Joshi HC and Archer DR (2004) Noscapine crosses the blood-brain barrier and inhibits glioblastoma growth. *Clin Cancer Res* 10:5187-5201.

Landen JW, Lang R, McMahon SJ, Rusan NM, Yvon AM, Adams AW, Sorcinelli MD, Campbell R, Bonaccorsi P, Ansel JC, Archer DR, Wadsworth P, Armstrong CA and Joshi HC (2002) Noscapine alters microtubule dynamics in living cells and inhibits the progression of melanoma. *Cancer Res* 62:4109-4114.

Lee D-U (2002) (-)-β-Narcotine: a facile synthesis and the degradation with ethyl chloroformate. *Bull Korean Chem Soc* 23:1548-1552.

Mikhailov A, Rieder CL (2002) Cell cycle: stressed out of mitosis. *Curr Biol* 12:R331-333.

Monzo M, Rosell R, Sanchez JJ, Lee JS, O'Brate A, Gonzalez-Larriba JL, Alberola V, Lorenzo JC, Nunez L, Ro JY and Martin C (1999) Paclitaxel resistance in non-small-cell lung cancer associated with beta-tubulin gene mutations. *J Clin Oncol* 17:1786-1793.

Morgan SE, Kim R, Wang PC, Bhat U, Kusumoto H, Lu T and Beck WT (2000) Differences in mutant p53 protein stability and functional activity in teniposide-sensitive and -resistant human leukemic CEM cells compared with parental CEM cells. *Oncogene* 19:5010-5019.

Pace A, Bove L, Nistico C, Ranuzzi M, Innocenti P, Pietrangeli A, Terzoli E, and Jandolo B (1996) Vinorelbine neurotoxicity: clinical and neurophysiological findings in 23 patients. *J Neurol Neurosurg Psychiatry* 61:409-411.

Panda D, Chakrabarti G, Hudson J, Pigg K, Miller HP, Wilson L and Himes RH (2000) Suppression of microtubule dynamic instability and tread milling by deuterium oxide. *Biochemistry* 39:5075-5081.

Panda D, Singh JP and Wilson L (1997) Suppression of microtubule dynamics by LY290181. *J Biol Chem* 272:7681-7687.

Peyrot V, Leynadier D, Sarrazin M, Briand C, Menendez M, Laynez J and Andreu JM (1992) Mechanism of binding of the new antimitotic drug MDL 27048 to the colchicine site of tubulin: equilibrium studies. *Biochemistry* 31:11125-11132.

Peyrot V, Leynadier D, Sarrazin M, Briand C, Rodriquez A, Nieto JM and Andreu JM (1989) Interaction of tubulin and cellular microtubules with the new antitumor drug MDL 27048. A powerful and reversible microtubule inhibitor. *J Biol Chem* 264:21296-21301.

Ranganathan S, Dexter DW, Benetatos CA, Chapman AE, Tew KD and Hudes GR (1996) Increase of beta(III)- and beta(IVa)-tubulin isotypes in human prostate carcinoma cells as a result of estramustine resistance. *Cancer Res* 56:2584-2589.

Rowinsky EK (1997) The development and clinical utility of the taxane class of antimicrotubule chemotherapy agents. *Annu Rev Med* 48:353-374.

Sammak PJ and Borisy GG (1987) Direct observation of microtubule dynamics in living cells. *Nature* 332:724-726.

Skehan P, Storeng R, Scudiero D, Monks A, McMahon J, Vistica D, Warren JT, Bokesch H, Kenney S and Boyd MR (1990) New colorimetric cytotoxicity assay for anticancer-drug screening. *J Natl Cancer Inst* 82:1107-1112.

Theiss C and Meller K (2000) Taxol impairs anterograde axonal transport of microinjected horseradish peroxidase in dorsal root ganglia neurons in vitro. *Cell Tissue Res* 299:213-224.

Topp KS, Tanner KD, and Levine JD (2000) Damage to the cytoskeleton of large diameter sensory neurons and myelinated axons in vincristine-induced painful peripheral neuropathy in the rat. *J Comp Neurol* 424:563-576.

Ye K, Ke Y, Keshava N, Shanks J, Kapp JA, Tekmal RR, Petros J and Joshi HC (1998) Opium alkaloid noscapine is an antitumor agent that arrests metaphase and induces apoptosis in dividing cells. *Proc Natl Acad Sci USA* 95:1601-1606.

Ye K, Zhou J, Landen JW, Bradbury EM, Joshi HC (2001) Sustained activation of p34(cdc2) is required for noscapine-induced apoptosis. *J Biol Chem* 276:46697-46700.

Zhou J, Panda D, Landen JW, Wilson L and Joshi HC (2002a) Minor alteration of microtubule dynamics causes loss of tension across kinetochore pairs and activates the spindle checkpoint. *J Biol Chem* 277:17200–17208.

Zhou J, Gupta K, Yao J, Ye K, Panda D, Giannakakou P and Joshi HC (2002b) Paclitaxel-resistant human ovarian cancer cells undergo c-Jun $NH_2$-terminal kinase-mediated apoptosis in response to noscapine. *J Biol Chem* 277:39777-39785.

Zhou J, Gupta K, Aggarwal S, Aneja R, Chandra R, Panda D and Joshi HC (2003) Brominated derivatives of noscapine are potent microtubule-interfering agents that perturb mitosis and inhibit cell proliferation. *Mol Pharmacol* 63:799–807.

Zhou J, Liu M, Aneja R, Chandra R, Joshi HC (2004) Enhancement of paclitaxel-induced microtubule stabilization, mitotic arrest, and apoptosis by the microtubule-targeting agent EM012. *Biochem Pharmacol* 68:2435-2441.

Zhou J, Giannakakou P (2005) Targeting microtubules for cancer chemotherapy. *Curr Med Chem Anticancer Agents* 5:65-71.

Zhou J, Liu M, Luthra R, Jones J, Aneja R, Chandra R, Tekmal RR, Joshi HC (2005a) EM012, a microtubule-interfering agent, inhibits the progression of multidrug-resistant human ovarian cancer both in cultured cells and in athymic nude mice. *Cancer Chemother Pharmacol* 55:461-5.

Molecular Pharmacology Fast Forward. Published on March 3, 2006 as DOI: 10.1124/mol.105.021899
This article has not been copyedited and formatted. The final version may differ from this version.


**Footnotes**

This work was supported by funding from the National Institutes of Health (to H.C.J.) and partly from the Department of Biotechnology, India (to D.P.).

Molecular Pharmacology Fast Forward. Published on March 3, 2006 as DOI: 10.1124/mol.105.021899
This article has not been copyedited and formatted. The final version may differ from this version.


**Figure Legends**

**Figure 1**. **A.** Synthesis of 9-nitro-noscapine. 9-nitro-nos was synthesized by the aromatic nitration of noscapine using silver nitrate in acetonitrile and TFAA at 25°C. **B.** 9-nitro-nos binds tubulin. Panel B shows the fluorescence quenching spectrum of tubulin for 9-nitro-nos. Control (■), 10 μM (●), 20 μM (▲), 50 μM (▼), 75 μM (♦), and 100 μM (○) of 9-nitro-nos. Panel C shows the double reciprocal plot which gives a dissociation constant ($K_d$) of 86 ± 6 μM for 9-nitro-nos binding to tubulin. 9-nitro-nos does not significantly change the polymerization rate and the steady state polymer mass of purified tubulin *in vitro* (Panel D). The assay was based on the light scattering ability of tubulin polymer, reflected as the absorbance at 550 nm wavelength. An equivalent amount of the solvent DMSO was used as a negative control. Control (■), 25 μM 9-nitro-nos (●), and 100 μM 9-nitro-nos (▲). Results are representative of four independent experiments performed.

**Figure 2.** 9-nitro-nos actively inhibits the proliferation of various human cancer cells including those that are resistant to vinblastine, teniposide and paclitaxel. CEM, CEM/VLB100, CEM/VM-1-5, 1A9, 1A9/PTX22 cells were treated with 9-nitro-nos at gradient concentrations for 72 hours. The $IC_{50}$ value, which stands for the drug concentration needed to prevent cell proliferation by 50% was then measured using standard *in vitro* proliferation assays. The 3-(4,5-dimethylthiazol-2-yl)-5-(3-carboxymethoxyphenyl)-2-(4-sulphophenyl)-2H-tetrazolium salt (MTS) assay was used for non-adherent suspension cells (CEM, CEM/VLB100 and CEM/VM-1-5) and the sulforhodamine B (SRB) assay was performed for adherent cells (1A9 and 1A9/PTX22). Each value represents average of two independent experiments with five replicates each.

**Figure 3**. 9-nitro-nos arrests the cell cycle at G2/M phase in human cancer cells. **A** and **B** represent the % G2/M and % sub-G1 cells as a function of time of treatment with 9-nitro-nos. Panels **C-G** clearly show an increase in the population of cells with degraded DNA (sub-G1 amount in the far left) in the three-dimensional fluorescence activated cell sorting analysis (FACS) of DNA amounts. Panel **H** shows the effect of 9-nitro-nos on the cell cycle profile of normal primary fibroblast cells. Even concentrations as high as 100 μM, did not alter the cell cycle progression profile of normal human cells. All cells were harvested for analysis at the indicated times, stained with propidium iodide and analyzed by flow cytometry (FACS) using the Cell Quest Software. The x-axis shows intensity of PI-fluorescence which is indicative of the total DNA content of cells in different phases of the cell cycle. The y-axis represents the number of cells in each phase of the cell cycle and the z-axis shows the time points viz. 0, 24, 48 and 72 hours. Results are representative of three experiments performed in triplicate.

Molecular Pharmacology Fast Forward. Published on March 3, 2006 as DOI: 10.1124/mol.105.021899
This article has not been copyedited and formatted. The final version may differ from this version.


**Figure 4**. 9-nitro-nos kills cancer cells by inducing apoptosis. This is revealed by major changes in the nuclear morphology of these cells. **A.** Top panel shows untreated cells that display normal microtubule arrays. 9-nitro-nos treatment for 72 hours completely changes the morphologies as seen by the fragmented condensed apoptotic bodies (**A**, bottom panel). *(Scale bar = 20 μM).* **B.** The fragmented DNA in the terminal stages of apoptosis was measured using a flow-cytometry based quantitative terminal deoxynucleotidyl transferase (TdT)-mediated bromo-deoxyuridine triphosphate (BrdUTP) reaction (TUNEL assay) in a representative cell line (1A9/PTX22). Untreated control cells (lower panel) and 50 μM 9-nitro-nos treated 1A9/PTX22 cells (upper panel). After 72 hours of 9-nitro-nos treatment, cells were processed for apoptosis by a flow cytometry-based TUNEL assay. The fragmented DNA was also visualized using confocal microscopy as an abundance of TUNEL-positive cells (upper right panel, open arrowhead). Untreated control cells appear red (lower right panel, solid arrowhead) (*Scale bar = 20 μM).* Data shown are from a representative experiment of two experiments performed. **C**. 9-nitro-nos treatment causes activation of caspase-3. *Panel* shows the time-dependent increase in caspase-3 activity on 9-nitro-nos treatment in CEM, CEM/VLB100, CEM/VM-1-5, 1A9 and 1A9/PTX22 cells. After drug incubation, caspase-3 activity was analyzed using the luminogenic substrate Z-DEVD-aminoluciferin.

Molecular Pharmacology Fast Forward. Published on March 3, 2006 as DOI: 10.1124/mol.105.021899
This article has not been copyedited and formatted. The final version may differ from this version.


**Table 1**. Effect of 9-nitro-nos on cell cycle progression of drug-resistant cell lines and their normal counterparts

| Cell cycle parameters, % | CEM | | | | CEM/VLB100 | | | | CEM/VM-1-5 | | | | 1A9 | | | | 1A9/PTX22 | | | |
|---|---|---|---|---|---|---|---|---|---|---|---|---|---|---|---|---|---|---|---|---|
| | 0 h | 24 h | 48 h | 72 h | 0 h | 24 h | 48 h | 72 h | 0 h | 24 h | 48 h | 72 h | 0 h | 24 h | 48 h | 72 h | 0 h | 24 h | 48 h | 72 h |
| $G_0/G_1$ | 45.5 | 24.8 | 19.7 | 13.9 | 46.9 | 25.5 | 23.7 | 8.7 | 36.0 | 25.4 | 13.7 | 10.5 | 50.0 | 30.6 | 28.6 | 16.7 | 57.0 | 27.3 | 5.9 | 14.1 |
| S | 25.0 | 10.0 | 8.1 | 8.9 | 17.6 | 17.7 | 9.3 | 4.5 | 19.4 | 13.0 | 11.0 | 8.7 | 21.8 | 14.3 | 10.6 | 9.6 | 8.8 | 4.7 | 3.4 | 5.7 |
| $G_2/M$ | 20.9 | 34.2 | 40.0 | 16.9 | 25.7 | 36.0 | 30.2 | 12.5 | 30.7 | 41.0 | 15.0 | 12.2 | 21.2 | 34.2 | 17.2 | 9.0 | 20.4 | 31.4 | 44.3 | 13.7 |
| Sub-$G_1$ | 0.25 | 6.5 | 23.8 | 44.3 | 3.6 | 14.8 | 30.7 | 56.1 | 3.4 | 18.8 | 58.0 | 63.0 | 0.7 | 12.0 | 38.0 | 56.3 | 3.5 | 30.0 | 44.6 | 59.0 |

Cells were treated with 9-nitro-nos for the indicated time (hours) before being stained with propidium iodide for cell cycle analysis

# Figure 1

A

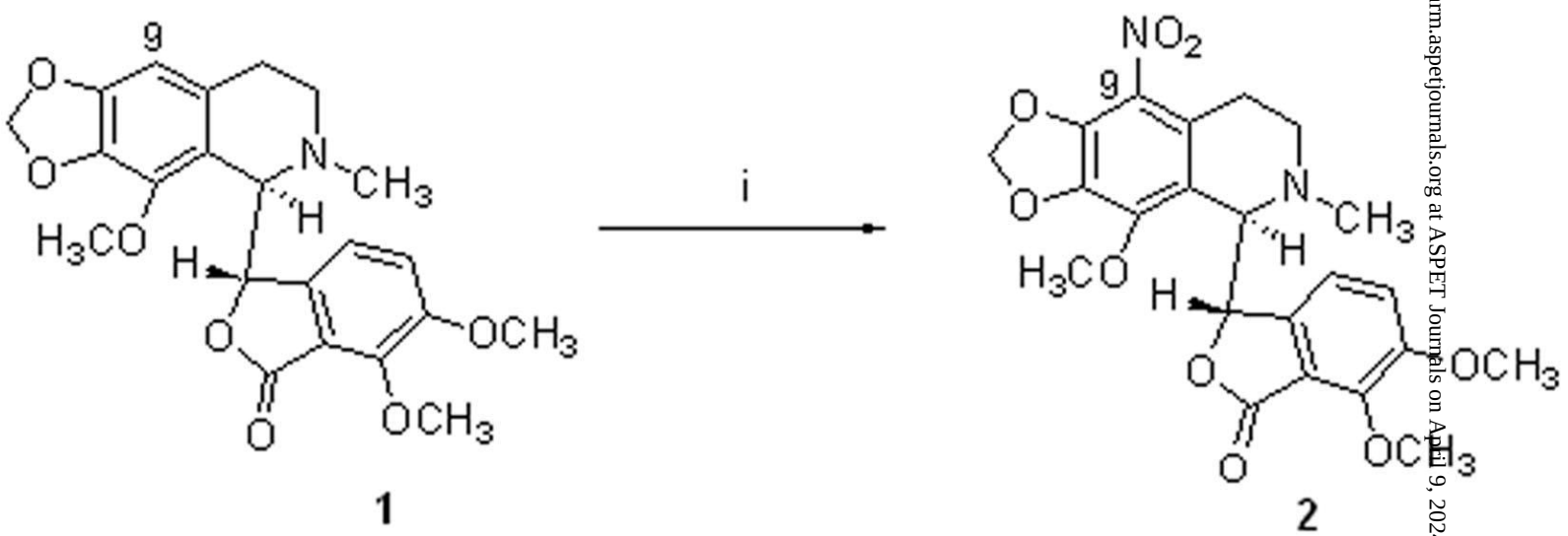


1 2

Reagents and Conditions: (i) $AgNO_3$, TFAA, ACN, 25$^{O}$C, 1 hour



B

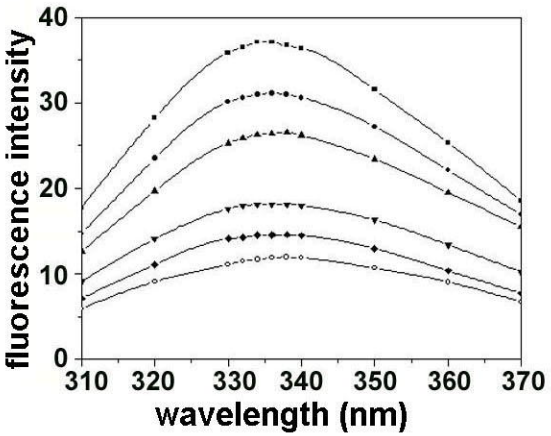


C

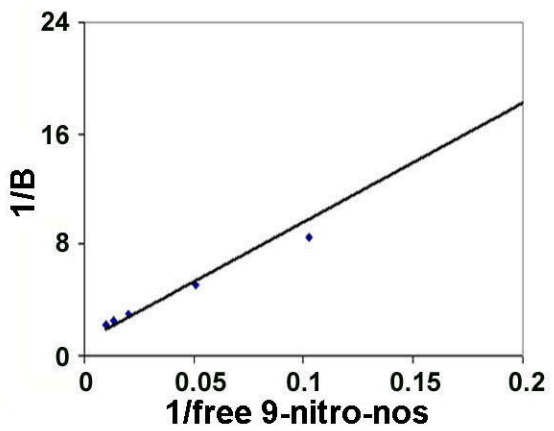


D

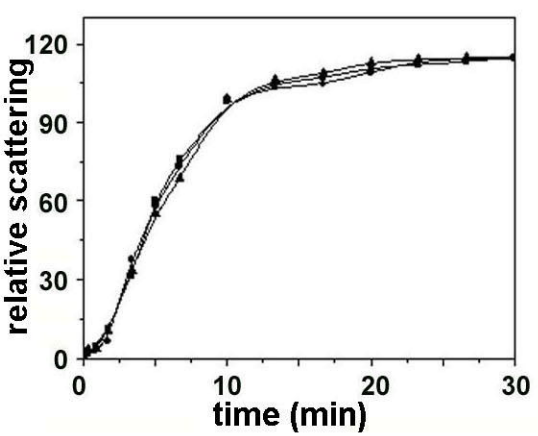

Figure 2

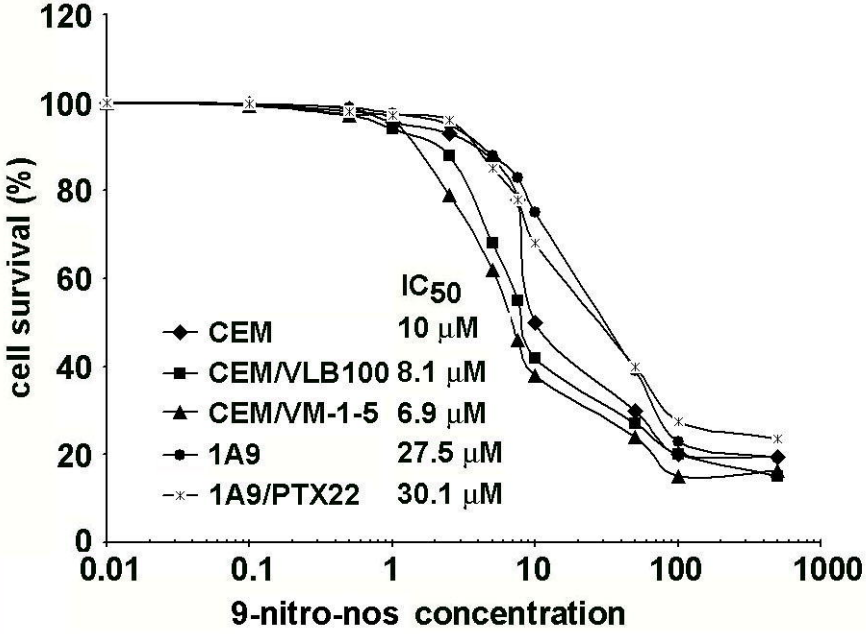
120
100
80
60
40
20
0
cell survival (%)
0.01
0.1
1
10
100
1000
9-nitro-nos concentration
IC50
CEM 10 μM
CEM/VLB100 8.1 μM
CEM/VM-1-5 6.9 μM
1A9 27.5 μM
1A9/PTX22 30.1 μM

# Figure 3

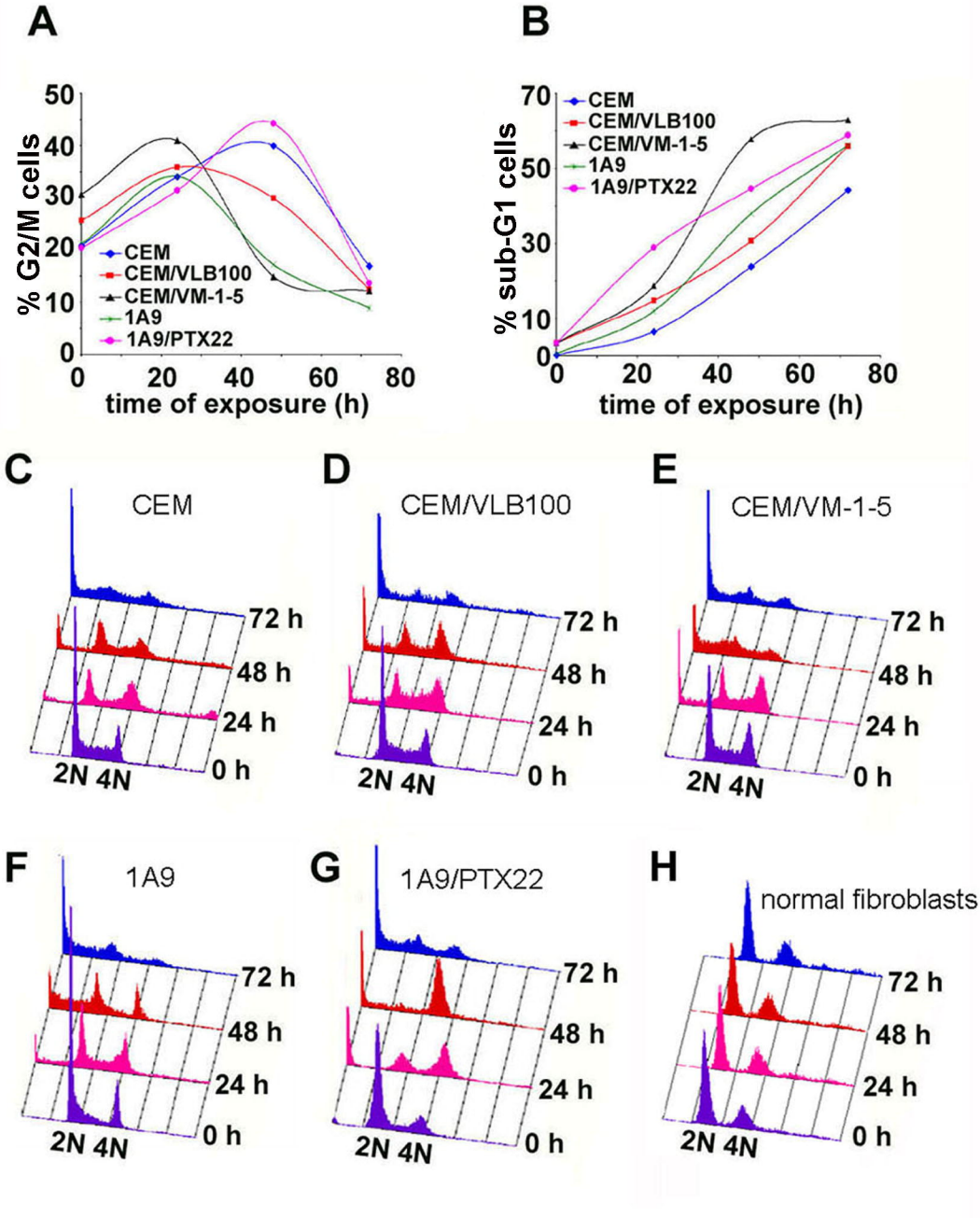
A
% G2/M cells
time of exposure (h)
CEM
CEM/VLB100
CEM/VM-1-5
1A9
1A9/PTX22
B
% sub-G1 cells
time of exposure (h)
C
CEM
D
CEM/VLB100
E
CEM/VM-1-5
F
1A9
G
1A9/PTX22
H
normal fibroblasts
72 h
48 h
24 h
0 h
2N 4N

Figure 4

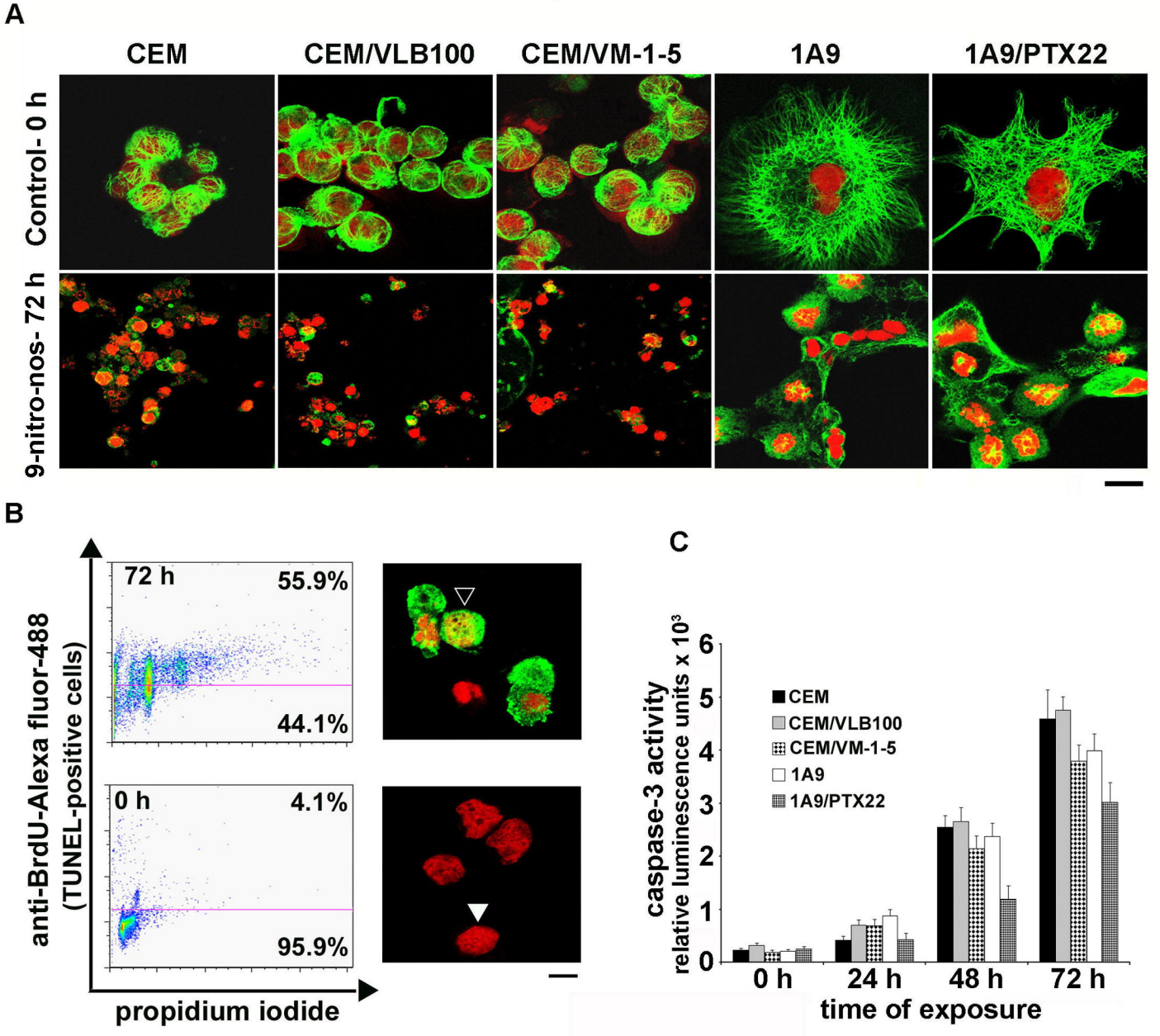
A
CEM
CEM/VLB100
CEM/VM-1-5
1A9
1A9/PTX22
Control- 0 h
9-nitro-nos- 72 h
B
72 h
55.9%
44.1%
0 h
4.1%
95.9%
anti-BrdU-Alexa fluor-488
(TUNEL-positive cells)
propidium iodide
C
caspase-3 activity
relative luminescence units x 10³
CEM
CEM/VLB100
CEM/VM-1-5
1A9
1A9/PTX22
0 h
24 h
48 h
72 h
time of exposure